Molecular Vision 2025; 31:99-112 <http://www.molvis.org/molvis/v31/99>
Received 7 August 2024 | Accepted 26 March 2025 | Published 28 March 2025

Astragaloside IV improves the survival rates of retinal ganglion cells in traumatic optic neuropathy by regulating autophagy mediated by the AMPK-MTOR-ULK signaling pathway

Wu Sun,[1,2] Guojun Chao,[3] Qiong Wu,[4] Yanting Xia,[5] Mengqiu Shang,[5,3] Qiping Wei,[5] Jian Zhou,[2,5] Liang Liao[2,5]

[1]Department of Ophthalmology, Xiyuan Hospital China Academy of Chinese Medical Sciences, Beijing, China; [2]Beijing University of Chinese Medicine, Beijing, China; [3]Eye Hospital, Chinese Academy of Chinese Medical Sciences, Beijing, China; [4]Beijing Tongren Hospital, Beijing, China; [5]Department of Ophthalmology, Dongfang Hospital, Beijing University of Chinese Medicine, Beijing, China

Purpose: Autophagy is involved in the pathological changes of traumatic optic neuropathy (TON), and the regulation of autophagy mediated by the AMPK-mTOR-ULK pathway is a potential therapeutic approach. Astragaloside IV (AS-IV) can regulate autophagy and play a therapeutic role in various diseases. This study aimed to observe the therapeutic effect of astragaloside on TON and the role of AMPK-MTOR-ULK pathway-mediated autophagy in this process.

Methods: After the TON model was established, varying doses of AS-IV were administered as an intervention. Additionally, compound C (an AMPK inhibitor) or 3-methyladenine (an autophagy inhibitor) was administered intraperitoneally in conjunction with AS-IV. Samples were collected following a 7-day intervention period. Western blot analysis was conducted to measure the protein and phosphorylation levels of AMPK, mTOR, and ULK proteins. Moreover, western blot and quantitative reverse transcription PCR assays were used to quantify LC3 levels in retinal tissue. LC3 immunofluorescence was performed to examine autophagy levels in the ganglion cell layer (GCL), while transmission electron microscopy was employed to observe autophagosomes. Additionally, BRN3A immunofluorescence was used to label retinal ganglion cells (RGCs) in the GCL, and terminal deoxynucleotidyl transferase dUTP nick-end labeling staining was used to assess apoptosis within the GCL. Finally, optic nerve conduction function was evaluated using flash visual evoked potentials.

Results: After 7 days, the phosphorylation levels of AMPK, mTOR, and ULK proteins in retinal tissue exhibited significant changes following TON. AS-IV treatment enhanced LC3 messenger RNA and protein levels in TON model rats, and the autophagy-promoting effect of AS-IV was reversed by 3-methyladenine. Moreover, AS-IV elevated P-AMPK and P-ULK levels while decreasing P-mTOR levels. AS-IV also improved the survival rate of RGCs and reduced the P2 peak latency of flash visual evoked potentials. These effects were attenuated by the AMPK inhibitor compound C. Additionally, AS-IV increased the levels of AKT1 and P-AKT1 while decreasing P-S6RP levels in the retinal tissue of TON model rats.

Conclusions: AS-IV can increase the survival rate of RGCs and improve visual function after TON, which may be related to the improvement of autophagy by regulating the AMPK-MTORC1-ULK pathway.

Traumatic optic neuropathy (TON) is a category of acute optic nerve injury usually caused by orbital, ocular, or cephalofacial trauma that can lead to severe irreversible vision loss [1]. Primary injuries caused by direct external forces can result in the destruction of the optic nerve capsule, partial or complete transection of the optic nerve, and impaired blood supply to the central region of the optic nerve. Subsequent secondary injury can initiate a series of biochemical cascades, leading to optic nerve ischemia and hypoxia, which lead to inflammation, immune responses, excitatory toxicity, oxidative damage, and ultimately oligodendrocyte apoptosis caused by axon demyelination and retinal ganglion cell (RGC) apoptosis [2]. Existing evidence shows that neither hormone therapy nor optic canal decompression provides additional benefit to patients compared to observation alone [3,4]. Exploring the mechanisms of RGC survival after optic nerve injury and improving RGC survival are important research strategies for the treatment of TON [5].

Numerous reports have outlined the role of autophagy in RGC death following TON [5-8]. After intravitreal injection of the autophagy inhibitor 3-methyladenine (3-MA), the number of microtubule-associated protein 1 light chain 3-II (LC3-II)–positive autophagosomes in the rat retina decreased, resulting in a significant delay in the acute phase of axonal degeneration following optic nerve crush [9]. Similarly, Atg4B$^{-/-}$ mice, which lack autophagy genes, show no significant differences in retinal function compared to wild-type

Correspondence to: Liang Liao, Department of Ophthalmology, Dongfang Hospital, Beijing University of Chinese Medicine, 6 Fangxingyuan, Fengtai District, Beijing 100078, China; Phone: +86 134 6637 9490; email: b00993@bucm.edu.cn

mice under normal physiologic conditions but display more severe retinal function impairment after injury [10,11]. These findings indicate that autophagy deficiency or inhibition can exacerbate damage to RGCs in TON. Conversely, the use of autophagy activators improved the survival rate of RGCs in TON models [10]. Therefore, these studies confirm that autophagy is involved in the process of RGC death and TON repair, suggesting that modulating the autophagic response might be a potential therapeutic approach for enhancing RGC survival following TON [12-14].

Among the various signaling pathways involved in autophagy, the AMPK-mTOR-ULK pathway has garnered significant attention [15]. Adenosine monophosphate-activated kinase (AMPK) is a critical enzyme highly conserved through evolution. Acting as a "cell energy sensor," its activity is influenced by adenosine monophosphate (AMP) levels [16]. Under normal conditions, the AMP level in cells is low, resulting in AMPK remaining in an inactive, dephosphorylated state. However, when RGCs experience energy deficiency due to axoplasmic flow block, the adenosine triphosphate content decreases, and the AMP level increases. The rise in the AMP/adenosine triphosphate ratio activates AMPK, which in turn triggers downstream signaling pathways to induce autophagy [16,17]. Previous studies have identified phosphorylated AMPK in optic nerve axons [18,19], and the AMPK activator A769662 has been shown to provide axonal protection by enhancing autophagy in tumor necrosis factor–induced optic nerve degeneration [19]. The mammalian target of rapamycin (mTOR), a member of the phosphatidylinositol kinase-related kinase family, is a crucial regulator of autophagy. mTOR exists in two distinct complexes: mTOR complex 1 (mTORC1), which is rapamycin sensitive, and mTOR complex 2 (mTORC2), which is relatively rapamycin insensitive [15]. In TON models, numerous studies have demonstrated that mTOR inhibitors improve the survival of RGCs [8-10]. Unc-51-like kinase (ULK) is a homolog of Atg1, an essential autophagy-related gene in mammals. ULK is the only core autophagy protein with serine/threonine kinase activity. Both mTOR and AMPK catalyze or inhibit the phosphorylation of ULK, thereby promoting or inhibiting autophagy, respectively [15-18]. Given that severe axonal injury leads to disrupted axoplasmic flow in RGCs and subsequent energy supply impairments, AMPK-mTOR-ULK–mediated autophagy might be a key pathophysiological mechanism affecting RGC survival.

Astragaloside IV (AS-IV) is the main active ingredient of the traditional Chinese medicine *Astragalus membranaceus*, known for its diverse functions, including oxygen free radical scavenging, anti-inflammatory effects, immunity enhancement, and cardiovascular improvement [20]. The regulatory effect of AS-IV on autophagy has been increasingly reported, but the results are inconsistent. Some studies have found that AS-IV can inhibit autophagy [21,22], while in other studies, AS-IV exerts its therapeutic effect by promoting autophagy [23-25]. To date, no research has examined the effects of AS-IV on traumatic optic nerve injury. Besides, AS-IV has been shown to regulate AMPK and mTOR proteins [26-29]. This study aims to explore the effect of AS-IV on the RGC survival rate in a TON animal model, as well as the potential role of the AMPK-mTOR-ULK autophagy pathway in this process.

METHODS

Ethics statement: Animal care and experiments were approved by the Bioethics Committee of Dongfang Hospital, Beijing University of Chinese Medicine (No. 202007). This experiment was performed in strict accordance with the regulations in the National Institutes of Health guidelines for animal care and use and the Association for Research in Vision and Ophthalmology Statement for the Use of Animals in Ophthalmic and Vision Research.

Materials: The following materials were purchased for this study: AS-IV (B20564; Shanghai Yuanye Biotechnology Co., Ltd., Shanghai, China), rapamycin (ab146591; Abcam, Cambridge, UK), compound C (dorsomorphin, ab120843; Abcam), LC3B (E5Q2K) mouse mAb (83506S; CST, Boston, MA), AMPKα (D63G4) rabbit mAb (40308ES20; CST), mTOR (7C10) rabbit mAb (2983S; CST), ULK1 (D8H5) rabbit mAb (8054S; CST), anti-phospho-AMPKα (Thr172) rabbit mAb (50081S; CST), phospho-mTOR (Ser2448; D9C2) XP rabbit mAb (5536S; CST), phospho-ULK1 (Ser555; D7O6U) rabbit mAb (14202S; CST), anti-Brn3A antibody (ab245230; Abcam), rabbit anti-phospho-RPS6 (Ser240 + Ser244) polyclonal antibody (bs-3389R; Bioss, Beijing, China), rabbit anti-phospho-AKT1 (Ser473) polyclonal antibody (bs-12456R; Bioss), AKT monoclonal antibody (bsm-52010R; Bioss), 3-MA (HY-19312; Monmouth Junction, NJ), TUNEL Apoptosis Detection Kit (40308ES20; YEASEN, Shanghai, China), goat anti-mouse IgG-HRP (ab6789; Abcam), and goat anti-rabbit IgG-HRP (ab205718; Abcam).

Experimental animals: SPF male Wistar rats (Beijing Vital River Laboratory Animal Technology Co., Ltd., Beijing, China) weighing 180 ± 20 g were reared in an environment with controlled humidity and temperature, access to free eating and drinking, and a 12-h light/dark cycle. Modeling experiments were performed after a 1-week adaptation period. A total of 175 rats were randomly divided into 7 groups (n = 25): the low-dose AS-IV group (ASIV-L), middle-dose

AS-IV group (ASIV-M), high-dose AS-IV group (ASIV-H), sham operation group (SH), model group (MO), rapamycin (mTORC1 complex inhibitor) group (RA), and compound C (AMPK inhibitor) group (CC). The low-, middle-, and high-dose AS-IV groups were intraperitoneally injected with AS-IV immediately after modeling at a dose of 10/20/40 mg/kg/d (vehicle composition: 10% dimethyl sulfoxide [DMSO], 40% PEG300, 5% Tween-80, and 45% saline) [30,31]. The RA group was intraperitoneally injected with the autophagy activator rapamycin at a dose of 2 mg/kg/d (vehicle composition: 10% DMSO, 40% PEG300, 5% Tween-80, and 45% saline) [32,33], and the CC group was intraperitoneally injected with AS-IV (20 mg/kg/d) + compound C (1 mg/kg/d; vehicle composition: 10% DMSO, 40% PEG300, 5% Tween-80, and 45% saline) [34,35]. The SH and MO groups were intraperitoneally injected with a vehicle at 1 ml/100 g/d. All groups were treated once daily for 1 week and then euthanized for further analysis. In addition, 20 Wistar rats were divided into four groups: SH, MO, ASIV-M, and 3-MA (ASIV-M + 3-MA). The 3-MA group was administered with 3-MA (15 mg/kg, twice a week; DMSO as vehicle composition) via intraperitoneal injection half an hour after the ASIV-M intervention.

Establishment of the TON model: TON animal modeling was performed as in a previous study [36]. Specifically, the retina and blood vessels of the rat's fundus were examined directly with an ophthalmoscope (Olympus Co., Ltd., Tokyo, Japan) before surgery. Rats were anesthetized by intraperitoneal injection of 1% pentobarbital (60 mg/kg), and the operated eyes were coated with carbomer gel. After iodine disinfection, the skin was incised along the temporal orbital rim of the right eye under a stereomicroscope, and the orbital fascia was incised to expose the orbital bone edge. The supraorbital connective tissue was cleansed, and the obliquus rectus muscle was separated and directed toward the orbital apex until the optic nerve sheath was exposed. The optic nerve sheath was carefully separated to expose the optic nerve, which was then wrapped and knotted with a 6-0 polyester suture 2 mm behind the eyeball. One end of the suture was fixed, and the other end was connected with a transverse tensiometer. Then, the suture was then pulled perpendicular to the optic nerve with a tension of 0.3 N for 20 s. After surgery, the skin was sutured, erythromycin eye ointment was applied to the operated eye, and the rats were placed on an electric heating pad at 37 °C for recovery.

In the SH group, the nerve sheath was cut to expose the optic nerve without retraction. All experimental rats were operated with the right eye as the surgical eye and the left eye as the control eye.

Animal euthanasia and eye tissue sampling: After 7 days of intervention, the rats were killed by an overdose of anesthesia (1% pentobarbital, 120 mg/kg). The eye tissue was then extracted as follows: surgical curved forceps were used to gently pull the mouse bulbar conjunctiva in the 9-o'clock direction, and ophthalmic curved scissors were used to cut along the fornix of the mouse bulbar conjunctiva. The eyelid, periocular, and intraorbital tissues were separated. The eyeball was gently lifted outward and upward to expose the retrobulbar tissue carefully. The eyeball was removed by cutting the retrobulbar tissue along the curvature of the posterior surface of the eyeball with curved ophthalmic scissors. Excess muscle and fascial tissue outside the eye were removed. The eyes were then fixed in a centrifuge tube prefilled with approximately 10 times the volume of the eyeball with Davidson's fixative.

The steps of retinal tissue extraction are as follows: the freshly harvested eyeball tissue was transferred to ice for retinal tissue extraction. After performing anterior chamber puncture along the corneal limbus, ophthalmic surgical scissors were used to cut around the corneal limbus 0.5 mm behind the limbus. The corneal tissue was then removed. The lens and vitreous tissue were carefully removed, and then the neuroepithelial retinal tissue (appearing as a light-yellow villous structure) was gently peeled off with microforceps and transferred to cryovials. The tissue was placed into a liquid nitrogen tank and then moved to a −80 °C freezer for storage.

Western blot: Retinal tissues were removed from the ultralow temperature freezer (−82 °C), and each sample was lysed by adding 150 µl RIPA lysis buffer for 30 min on ice. The lysate was centrifuged at 16,000 ×g for 15 min at 4 °C, and the protein concentration was determined using a BCA protein assay kit. Equal amounts of proteins were loaded on a 10% sodium dodecyl sulfate–polyacrylamide gel electrophoresis gel and separated. The proteins were then transferred to a polyvinylidene fluoride membrane, blocked at room temperature for 2 h, and incubated with the corresponding primary antibodies (mouse anti-LC3B, rabbit anti-AMPK, rabbit anti-mTOR, rabbit anti-ULK1, rabbit anti–P-AMPK, rabbit anti–p-mTOR, rabbit anti–p-ULK1, rabbit anti-phospho-AKT1, rabbit anti-phospho-RPS6, mouse anti-AKT1) overnight at 4 °C. Then, the membrane was incubated with the corresponding horseradish peroxidase–conjugated secondary antibodies (anti-mouse IgG [1:1,000] and anti-rabbit IgG [1:1,000]) in a shaker at 37 °C for 2 h. Enhanced chemiluminescence was used to detect the immunoreactive proteins, and an automatic chemiluminescence analyzer (YPH Bio Co. Ltd., Beijing, China) was used for exposure, photos, and data analysis.

Quantitative real-time PCR: Retinal tissue was removed from the −82 °C ultralow temperature freezer, RNA was extracted with TRIzol reagent (TransGen Biotech Co. Ltd., Beijing, China), and complementary DNA first-strand synthesis was performed using the FastKing complementary DNA first-strand synthesis kit. Amplification was performed using a two-step method according to the instructions for the real-time PCR kit (TransGen Biotech Co. Ltd.). The forward/backward primers for LC3B and GAPDH were designed by Shanghai Jierui Bioengineering Co., Ltd. (Shanghai, China): LC3B, AAG ACC TTC AAA CAG CGC C/GCA GGC GCC TTC TAA TTA TC, and GAPDH, GAT GAC ATC AAG AAG GTG GTG/ACC CTG TTG CTG TAG CCA TAT TC. The amplified products were subjected to agarose gel electrophoresis, and the messenger RNA (mRNA) expression level was analyzed by a real-time fluorescent quantitative PCR instrument (Applied Biosystems, Waltham, MA). Primer specificity was evaluated by melting curve analysis, and the $2^{-\Delta\Delta Ct}$ method was employed to measure relative mRNA expression levels.

Hematoxylin and eosin staining: Fresh retinal tissue was fixed in 4% paraformaldehyde for 48 h and then dehydrated in a dehydrator with gradient alcohol. After paraffin embedding, the sections were sliced at a thickness of 4 μm. The pathological sections were baked in an oven at 65 °C for 2 h. The paraffin sections were deparaffinized and rehydrated, stained with hematoxylin and eosin, and sealed with neutral resin. The pathological changes of the retina were observed using an upright optical microscope (Nikon, Tokyo, Japan).

Immunofluorescence staining and imaging: Paraffin sections were deparaffinized and placed in a repair box containing citric acid antigenic repair buffer (pH 6.0) for antigen retrieval in a microwave oven. After rinsing the sections with PBS and adding the corresponding primary antibodies (mouse anti-LC3B and rabbit anti-Brn3a), the sections were flatly placed in a wet box and incubated overnight at 4 °C. The tissues were covered with the corresponding secondary antibodies and incubated for 50 min at room temperature in the dark. After rinsing the sections with PBS, the nuclei were counterstained with 4′,6-diamidino-2-phenylindole dye solution and incubated in the dark for 10 min at 25 °C. The sections were sealed with an antifluorescence quenching sealant and then visualized under an inverted fluorescence microscope (Nikon).

Terminal deoxynucleotidyl transferase dUTP nick-end labeling: Terminal deoxynucleotidyl transferase dUTP nick-end labeling (TUNEL) staining of fragmented DNA was performed on retina tissue using the One Step TUNEL Apoptosis Assay Kit (Yeasen, Shanghai, China). Fixative-soaked eyes were dehydrated with 30% sucrose and then frozen and sectioned at a thickness of 12 μm. Sections were rinsed three times with PBS and then incubated for 5 min at room temperature in PBS containing 0.5% Triton X-100. After rinsing three times with PBS, the TUNEL assay solution (500 μl assay solution consisting of 50 μl terminal deoxynucleotidyl transferase enzyme and 450 μl fluorescent labeling solution) was added to the tissue and incubated for 60 min at room temperature. The sections were rinsed with PBS and incubated with 4′,6-diamidino-2-phenylindole at 25 °C for 10 min and finally observed under a fluorescence microscope.

Preparation of samples for transmission electron microscope analysis: Fresh retinal tissue was trimmed to approximately 1 mm^3 and fixed with 2.5% glutaraldehyde at 4 °C. After immersion in 0.1 M phosphate buffer, the tissue was fixed with 1% osmium tetroxide fixative and washed again with 0.1 M phosphate buffer. Tissues were dehydrated by ethanol gradient in a refrigerator at 4 °C, embedded in the epoxy resin Epon812, and finally cured in an oven (overnight at 37 °C, 12 h at 45 °C, 48 h at 60 °C). Afterward, the tissue was sliced with ultramicrotome Lycra EMUC7 at a thickness of 70 nm and double stained with 2% uranyl acetate-lead citrate. A transmission electron microscope (TEM), HT7800 (80 kV), was used for observation and filming.

Flash visual evoked potentials: The rats were tested with flash visual evoked potentials (F-VEPs) after 7 days of intervention. After 12 h of dark adaptation, rats were fully anesthetized with 1% pentobarbital (50 mg/kg) by intraperitoneal injection. The pupils were dilated with compound tropicamide (Santen Pharmaceutical Co., Ltd., Tokyo, Japan), and then F-VEP was recorded with an electrophysiological tester (Roland Electronics Co., Ltd., Keltern, Germany). A filamentous silver-silver chloride electrode was used as the VEP acting electrode and placed subcutaneously at the midpoint of the connection between the roots of the ears. The reference electrode was placed in the mouth, and the grounding electrode was placed subcutaneously at the tail. While one eye was recorded, the other eye was covered by an opaque eyecup. The parameters of the electrophysiological tester were set as follows: light intensity, 3.0 $CD \cdot s \cdot m^2$; stimulation frequency, 1.0 Hz; waveform analysis time, 250 ms; and recording frequency band of bandpass amplifiers, 1–100 Hz. The number of waveform superimpositions was 100. The first negative peak of the waveform was defined as the N1 wave, the positive peak following the N1 wave was defined as the P1 wave, and the negative and positive peaks following the P1 wave were defined as the N2 wave and the P2 wave, respectively. Visual function was assessed by comparing the latency time (ms) and amplitude (μv) of the P2 wave in

each group of rats according to the International Society for Clinical Electrophysiology of Vision criteria [37-39].

Statistical analysis: All data were analyzed with Prism 8.0 (GraphPad Software, La Jolla, CA, USA), and measurement data were expressed as the mean ± standard deviation. Pairwise comparisons were performed by the Student *t* test. Analysis of variance and the Dunnett method were used to compare the model group with all other groups (excluding the CC group). Analysis of variance, along with the Tukey method, was used to compare between drug groups (ASIV-L, ASIV-M, ASIV-H, and RA group). The difference was considered statistically significant when $p < 0.05$.

RESULTS

Autophagy occurs in the optic nerve lateral retraction model: Hematoxylin and eosin staining was performed to observe the retinal structure. We observed that the retinal tissue of rats in the SH group had a clear hierarchy and dense structure, whereas the retinal nerve fiber layer of model rats was thinned and the number of RGCs was relatively reduced (Figure 1A). F-VEP was used to evaluate the visual function of rats. Compared with the SH group, rats in the MO group showed a decrease in N2P2 amplitude and prolongation of P2 latency as detected by F-VEP, indicating successful modeling (Figure 1B).

To verify that autophagy was activated in model rats, LC3 protein levels in the ganglion cell layer (GCL) were detected by immunofluorescence staining. The results showed that the LC3 protein level in the GCL of the MO group was significantly higher than that in the SH group on day 7 after modeling (Figure 1C). In addition, observing the retinal tissues with TEM, we found that there were almost no double-layered autophagosomes in the SH group rats, whereas the number of autophagosomes was increased in the retinal tissues of the model rats (Figure 1D). The above results suggested that autophagy was activated in the retina tissue of model rats.

AS-IV can improve the number of RGCs in model rats by promoting autophagy: Immunofluorescence staining was used to assess the number of Brn3a-labeled RGCs in the rat retina 7 days after modeling [40]. As shown in Figure 2A, the number of Brn3a-positive cells in the MO group was significantly reduced compared to the SH group. In addition, the number of Brn3a-positive cells was significantly increased in the ASIV-M, ASIV-H, and RA groups compared to the MO group but not in ASIV-L group. The differences in the number of RGCs among various doses of AS-IV were not statistically significant. Similarly, no statistically significant difference was observed between RA and any of the AS-IV groups. In addition, after intraperitoneal injection of

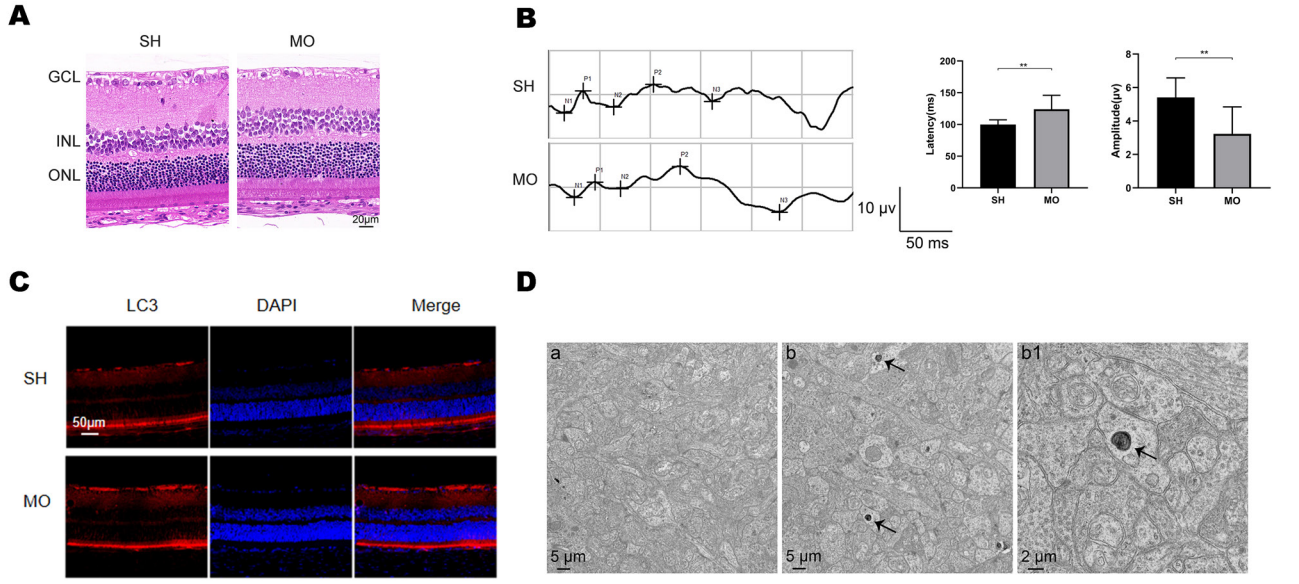

Figure 1. Autophagy occurs in the optic nerve lateral retraction model. **A**: Hematoxylin and eosin staining was used to observe the retinal tissue in the SH (sham operation) group and the MO (model) group. GCL, ganglion cell layer; INL, inner nuclear layer; ONL, outer nuclear layer. **B**: The changes in F-VEP in the SH and MO groups (n = 9). Mean ± standard deviation; **p < 0.01. **C**: Immunofluorescence staining was used to assess LC3 protein in the retinal tissues of the SH and MO groups. **D**: The retinal tissue of rats was observed under a transmission electron microscope. a, Normal retinal ultrastructure; b, retinal ultrastructure after 7 days in the model group, bar = 5 μm; b1, partially enlarged image b, bar = 2 μm. The arrow refers to the autophagosome.

compound C in conjunction with astragaloside IV, the number of RGCs was significantly reduced compared to the ASIV-M group ($p < 0.05$).

To study the regulation of autophagy by AS-IV, the effect of AS-IV on the expression of LC3B was observed in the retinal tissue of model rats. The western blot results showed that AS-IV increased the level of LC3-II/LC3-I in the retina compared with the MO group (all $p < 0.05$). In

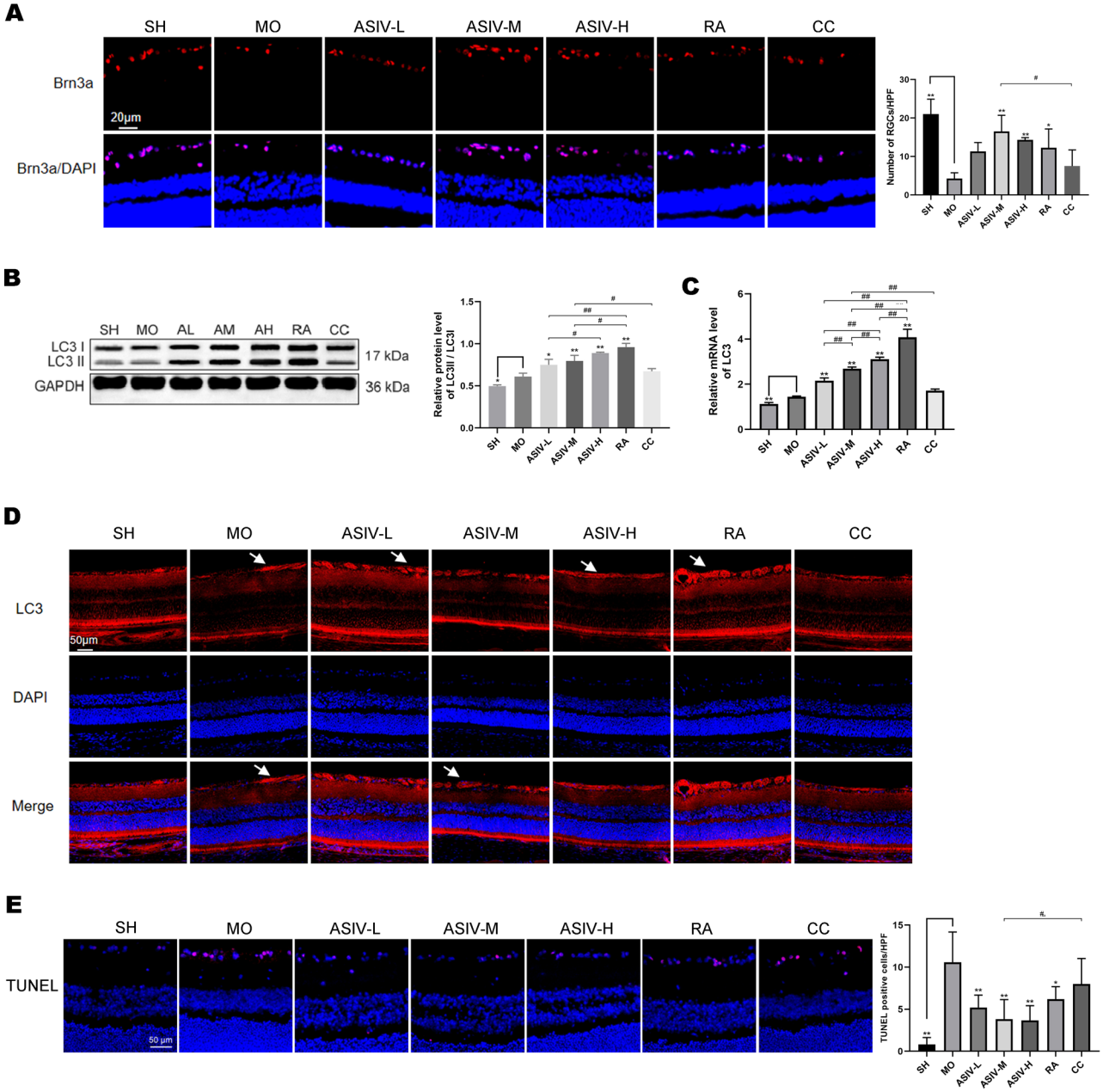

Figure 2. AS-IV can improve the number of RGCs in model rats by promoting autophagy. **A**. Brn3a immunofluorescence staining was used to label RGCs in the retinal tissues of rats in all groups ($n \geq 3$). **B**. Western blotting was used to assess LC3 protein levels in the retinal tissue of rats in all groups ($n = 3$). **C**. Real-time-PCR was used to assess the expression level of LC3 mRNA in the retina of rats in each group ($n = 9$). **D**. An immunofluorescence staining method was used to assess LC3 level in the retinal tissues of each group. **E**. TUNEL staining was used to label apoptotic cells (green) in the GCL ($n \geq 3$); arrows point to apoptotic cells. Mean ± standard deviation; *$p < 0.05$ or **$p < 0.01$, compared with the MO group (excluding the CC group); #$p < 0.05$, comparison between the drug groups.

addition, LC3-II/LC3-I levels in retinal tissue were increased in the ASIV-H group compared with the ASIV-L group ($p < 0.05$), while the difference between the ASIV-H and ASIV-M groups, as well as between the ASIV-M and ASIV-L groups, was not statistically significant (Figure 2B). Real-time PCR showed that AS-IV could promote the expression of LC3 mRNA compared with the MO group (all $p < 0.05$), and the level of LC3 mRNA was significantly increased in the ASIV-H group compared with the ASIV-M and ASIV-L groups (all $p < 0.05$). In addition, the difference between the ASIV-M and ASIV-L groups was also statistically significant (Figure 2C). LC3 immunofluorescence staining further showed that the LC3 expression levels in the GCL of the AS-IV group were significantly higher than that of the MO group (Figure 2D). In addition, the protein and mRNA levels of LC3 in the retinal tissues of rats in the RA group were higher than those in the MO group ($p < 0.05$).

To further confirm whether AMPK plays a role in autophagy regulation in AS-IV, an AMPK inhibitor (compound C) was used in the ASIV-M group. The results showed that after compound C intervention, LC3 protein and mRNA levels were significantly lower than those in the ASIV-M group (Figure 2B,C), and LC3 expression levels were also reduced in immunofluorescence staining (Figure 2D). The above results indicated that AS-IV could increase the autophagy level in the retinal tissues of model rats, and inhibition of AMPK could reduce this effect.

To further validate our findings, TUNEL staining was used to detect cell apoptosis in the GCL. As shown in Figure 2E, the number of apoptotic cells in the GCL was significantly higher in the model group than in all other groups except the CC group. In addition, the number of apoptotic cells in the GCL in the CC group was significantly higher than that in the ASIV-M group.

AS-IV enhances autophagy by regulating the phosphorylation of AMPK, mTOR, and ULK proteins: Western blot analysis was employed to evaluate the protein expression and phosphorylation levels of AMPK, mTOR, and ULK in the retinas of model rats (Figure 3A). The results indicated no significant differences in the protein expression levels of AMPK, mTOR, and ULK in the retinal tissues of the various groups, whereas there were significant differences in the phosphorylation levels of AMPK, mTOR, and ULK. Compared to the SH group, the MO group exhibited increased levels of P-AMPK and P-ULK and reduced levels of P-mTOR (all $p < 0.05$). Additionally, all the AS-IV groups, when compared to the MO group, exhibited higher levels of P-AMPK and P-ULK and lower levels of P-mTOR in retinal tissues (all $p < 0.05$). Furthermore, high-dose AS-IV significantly elevated P-AMPK and P-ULK levels while reducing P-mTOR levels compared to low-dose AS-IV. However, the differences among the ASIV-H, ASIV-M, and ASIV-L groups were not statistically significant.

After a week of intraperitoneal injection of compound C in the ASIV-M group, the levels of P-AMPK and P-ULK were observed to decrease in the retinal tissue ($p < 0.05$), whereas the levels of P-mTOR were significantly higher than those in the ASIV-M group ($p < 0.05$). Elevated phosphorylation of AMPK and ULK or decreased phosphorylation of mTOR can induce autophagy [15], and AS-IV increased the levels of P-AMPK and P-ULK and reduced P-mTOR levels in the retina of model rats. In summary, AS-IV can increase the autophagy level in the retina of model rats by regulating the phosphorylation of AMPK, mTOR, and ULK and may have a dose effect on the regulation of P-AMPK, P-mTOR, and P-ULK.

To further observe the regulatory effect of AS-IV on autophagy, we combined the use of the autophagy inhibitor 3-MA with ASIV intervention. The results showed that the LC3-II/LC3-I ratio in the 3-MA group significantly decreased compared to the ASIV-M group ($p < 0.05$), indicating that the use of 3-MA reversed the autophagy enhancement effect of ASIV (Figure 3B).

We further investigated the effects of AS-IV on mTOCR1 and mTORC2. The activity of mTORC1 was assessed by detecting p-RPS6 protein levels in retinal tissues [41,42], which was lower in the AS-IV group than in the MO group ($p < 0.05$; Figure 3C). In addition, mTORC2 activity was assayed by the p-AKT/AKT ratio [43] and was higher in the AS-IV group than in the MO group ($p < 0.05$).

AS-IV can improve the visual function of TON model rats: F-VEP was used to detect the ocular electrophysiological changes of the rats in each group after 7 days of intervention, and the latency time and amplitude of the P2 peak were used to evaluate the visual function of rats [38,39]. As shown in Figure 4, the P2 peak latency in the MO group was significantly longer than in the SH group ($p < 0.05$). Additionally, the AS-IV and RA groups exhibited shorter P2 peak latencies than the MO group (all $p < 0.05$). Furthermore, the P2 latency in the CC group was significantly longer than in the ASIV-M group ($p < 0.05$). However, no statistically significant difference in P2 latency was observed between the drug groups.

Regarding the amplitude of the N2P2 wave, a significant decrease was noted in the MO group compared to the SH group ($p < 0.05$), with no significant differences observed between the drug and MO groups. Moreover, there was no significant difference in N2P2 amplitude between the

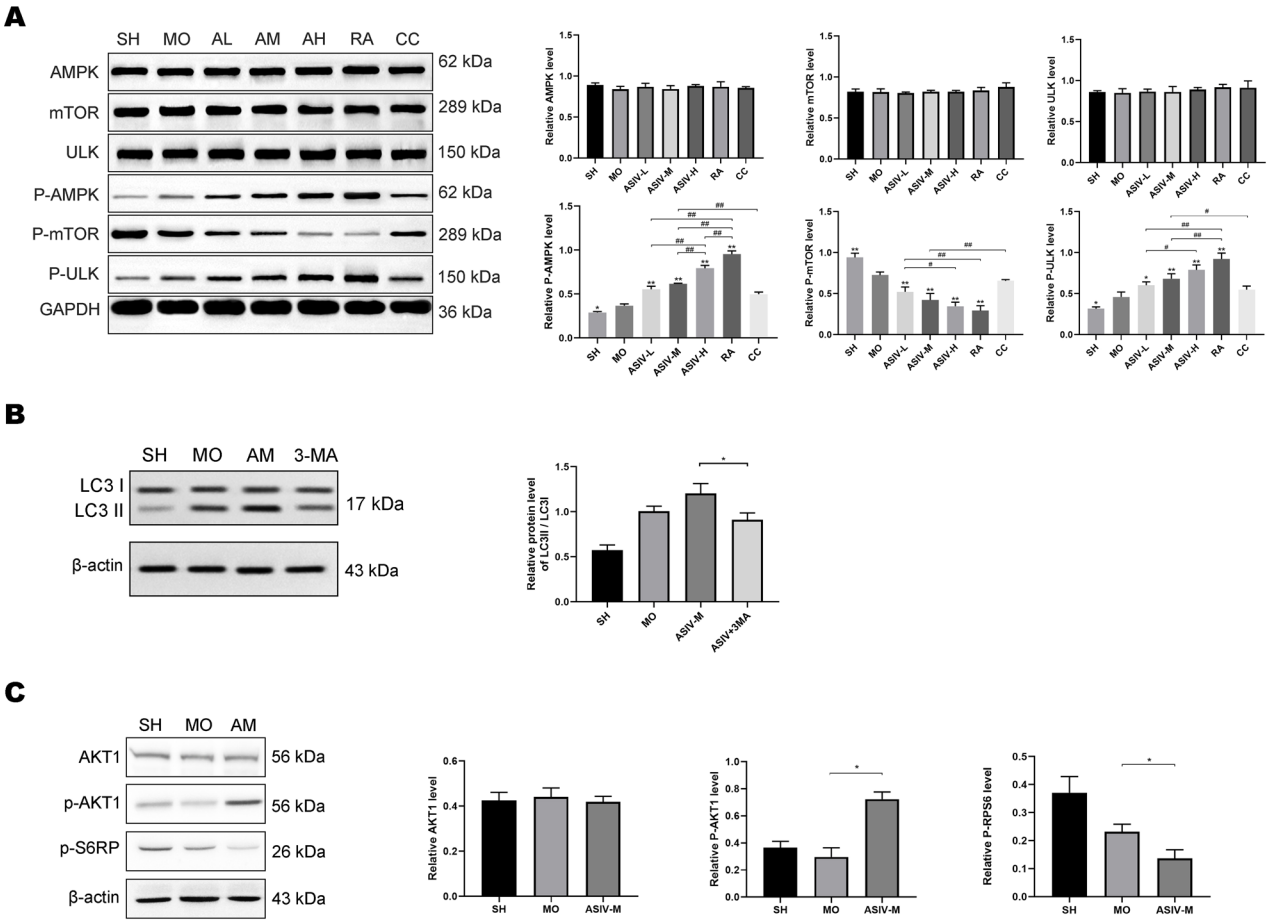

Figure 3. AS-IV enhances autophagy by regulating the phosphorylation of AMPK, mTOR, and ULK. **A**. Western blot was used to assess the AMPK, mTOR, and ULK phosphorylation levels in retinal tissue of rats in all groups ($n = 3$). *$p < 0.05$ or **$p < 0.01$, compared with the MO group (excluding the CC group). #$p < 0.05$ or ##$p < 0.01$, comparison between all drug groups. **B**. LC3 protein levels in retinal tissue ($n = 3$). *$p < 0.05$, comparison between AS-IV and 3-MA group. **C**. The AKT1 and S6RP phosphorylation levels in retinal tissue ($n = 3$); *$p < 0.05$, comparison between AS-IV and MO group.

ASIV-M and CC groups. Collectively, these findings indicate that AS-IV can improve the latency time of the P2 peak of F-EVP in TON model rats and that AMPK may play a key role in this process.

DISCUSSION

Our study found that the AMPK-mTOR-ULK signaling pathway is involved in the injury repair process of TON, and AS-IV could improve RGC survival by regulating autophagy increased by the AMPK-mTORC1-ULK pathway. In addition, AS-IV could improve the visual function of TON model rats through AMPK protein.

Astragalus is commonly used in China for the treatment of optic nerve disorders [44], and its main component, AS-IV, may play a major role in this process [45]. Several studies have reported that AS-IV plays a role in a variety of neurodegenerative diseases, including diabetic optic neuropathy and glaucoma [20,46-48]. However, no study has reported its effect on traumatic optic nerve injury. In this study, we found that AS-IV enhanced RGC survival in the TON model, which was reflected in the Brn3a immunofluorescence staining method and TUNEL staining (Figure 2). AS-IV has been reported to be involved in autophagy regulation in various diseases [20], but few studies have explored its role in regulating autophagy in the TON model. In this in vivo study, we found that AS-IV elevated the autophagy level in the retinal tissues of TON model rats (Figure 2 and Figure 3). Several studies have confirmed that autophagy improves RGC survival after TON [6,8,10], which is consistent with our results: the survival number of RGCs in the RA group was higher than that in the MO group. Thus, we hypothesized that

AS-IV may exert a pharmacological effect to protect RGCs by enhancing autophagy.

The AMPK-mTOR-ULK pathway is one of the key pathways mediating autophagy, and its role in optic nerve injury remains unclear. The RGC energy supply is restricted after optic nerve injury, and AMPK is activated as an energy receptor, as well as mTOR as a nutrient receptor. Therefore, we hypothesized that the AMPK-mTOR-ULK pathway may play a role in TON. In our study, we found no changes in the levels of AMPK, mTOR, and ULK proteins in the retinal tissues of the TON model, whereas their phosphorylation levels were altered after optic nerve clamping injury. AMPK can inhibit mTORC1 activity by phosphorylating the raptor protein of mTORC1, which in turn induces autophagy [15,17,49]. When cells are stimulated by starvation, activated AMPK phosphorylates the Ser555 site in ULK1/2, or ULK1/2 autophosphorylates and phosphorylates Atg13 and FIP200 to activate autophagy [15,50]. Considering that AMPK phosphorylation mediates autophagy and some studies have reported that autophagy protects the RGCs [9-11], we hypothesized that AS-IV may regulate autophagy through AMPK-mTOR-ULK and thus exerts a protective effect. We noted that the levels of AMPK, mTOR, and ULK proteins in the retinal tissues of TON model rats did not change significantly after AS-IV intervention, whereas their phosphorylation levels changed significantly. AS-IV was found to increase P-AMPK and P-ULK, as well as reduce P-mTOR levels (Figure 3). Previous studies have found that AS-IV regulates the AMPK protein. AS-IV has been found to induce the activation of AMPK in microglia in an ischemic stroke rat model [51] and to alleviate atorvastatin-induced hepatotoxicity by increasing AMPK phosphorylation levels in an atorvastatin-induced hepatotoxicity rat model [52]. In this study, AS-IV increased AMPK phosphorylation levels. Besides, the addition of an AMPK inhibitor resulted in decreased autophagy levels and a concomitant reduction

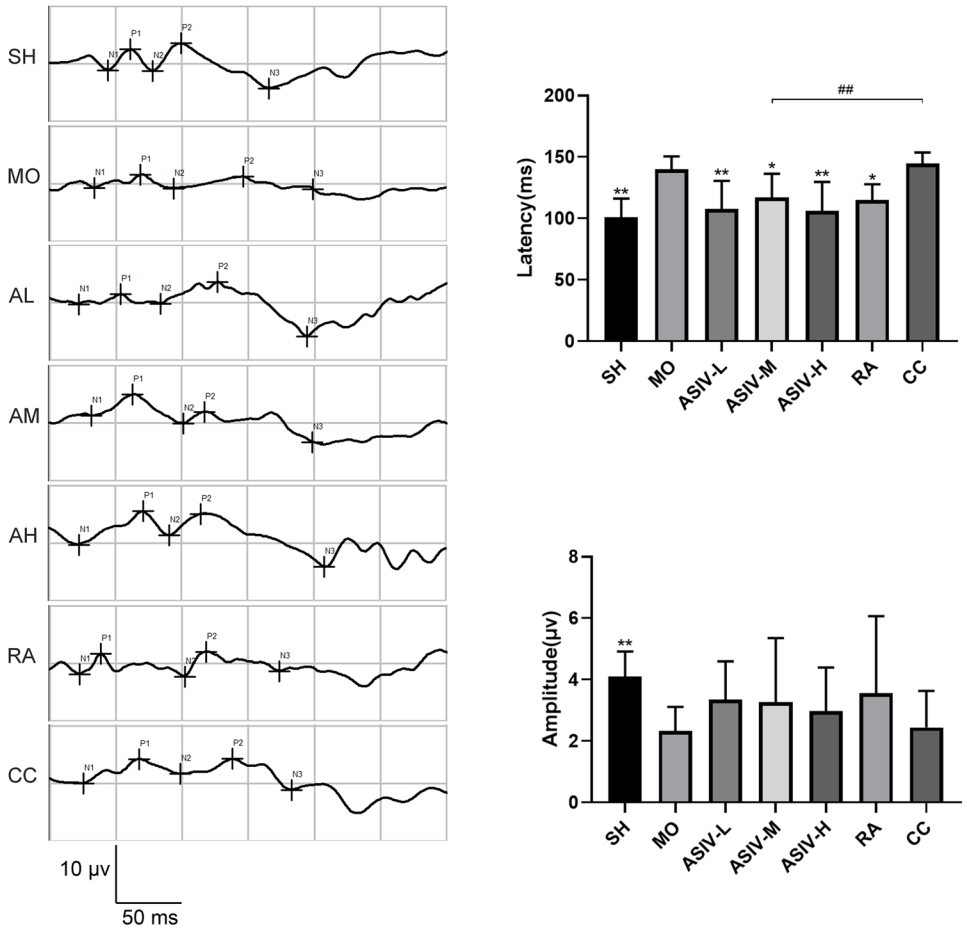

Figure 4. AS-IV improves visual function in TON model rats. Typical graphs of F-VEP of rats in all groups; mean ± standard deviation ($n = 9$); *$p < 0.05$ or **$p < 0.01$, compared with the MO group (excluding the CC group); #$p < 0.05$ or ##$p < 0.01$, comparison between all drug groups.

in the survival rate of RGCs (Figure 2 and Figure 3). We further used the autophagy inhibitor 3-MA to confirm that AS-IV regulates autophagy through AMPK phosphorylation. These results indicate that AS-IV exerts protective effects through AMPK-mediated autophagy. Increased AMPK phosphorylation can inhibit mTOR phosphorylation, increase ULK phosphorylation, and thereby activate autophagy [15]. Similar changes were observed in our results (Figure 3), suggesting that AS-IV could potentially regulate mTOR and ULK indirectly through AMPK. Additionally, AS-IV can directly inhibit mTOR phosphorylation levels [53] or indirectly inhibit mTOR phosphorylation levels through the PI3K and V-akt murine thymoma viral oncogene homolog (Akt) proteins [54,55], thereby promoting autophagy. These results suggest that AS-IV could play a role in the intricate regulatory network involving AMPK, mTOR, and ULK in the TON model.

As a complex of mTOR, both mTORC1 and mTORC2 are involved in the regulation of autophagy [15]. We further studied the effect of AS-IV on mTORC1 and mTORC2. Assessing the activity of mTORC1 by detecting p-RPS6 protein levels [41,42], we found that AS-IV inhibited the activity of mTORC1. In addition, the activity of mTORC2 was detected by the ratio of p-AKT/AKT [43], which was elevated in retinal tissues after AS-IV treatment. Decreased mTORC1 activity promotes autophagy, whereas an elevated p-AKT/AKT ratio inhibits autophagy [56,57]. The above results indicate that the autophagy-enhancing effect of AS-IV by inhibiting mTORC1 activity significantly exceeds the autophagy-inhibiting effect caused by the increasing activity of mTORC2, suggesting that AS-IV enhances autophagy by inhibiting the mTORC1 pathway. The elevated ratio of p-AKT/AKT is more likely to mediate the inhibition of apoptosis [58,59] and is reflected in our TUNEL results (Figure 2).

F-VEP was used to assess visual conduction function, which reflects the functional state activity from the retina to the visual cortex. F-VEP amplitude has been reported to reflect the number of functional optic nerve fibers [60,61]. However, we did not observe the improvement effect of AS-IV on the N2P2 amplitude. Variability in the amplitude of F-VEP detection may obscure the effect [62,63], although we controlled for this variability in several ways, controlling for dark adaptation, depth of anesthesia, implantation location, and depth of test electrodes; repeated external stimulation 100 times to minimize electroencephalogram noise [64]; and only included graphs with an error waveform less than 10 times. Interestingly, we found that AS-IV had the effect of improving P2 latency in F-VEP detection. The assessment of visual signal conductivity by VEP recording is a reliable tool for assessing the degree of demyelination of the visual pathway [50]. Previous studies have shown that the extended latency of VEP corresponds to the amount of demyelination in the visual pathway [61,65] and that autophagy can improve myelin regeneration and reduce neuronal degeneration [66,67]. Therefore, we speculated that AS-IV may promote the regeneration of the optic nerve myelin sheath by mediating autophagy, thereby improving the conduction function of the optic nerve. The P2 latency time was significantly shortened after rapamycin intervention in model rats, further verifying that autophagy was involved in the process of visual function repair after TON (Figure 4). Regrettably, we did not observe specific changes in the myelin sheath of the optic nerve, and the role of AS-IV on myelin sheath is still unclear. The pathological changes in the optic nerve myelin sheath after TON and the influence of autophagy on optic nerve myelin are worthy of further study.

Although our study has found the protective effect of AS-IV on RGCs in TON rats, some issues and limitations still need to be addressed and resolved in future research. This study determined that AS-IV exerts a protective effect on TON rats through autophagy, but the specific mechanism of how autophagy works remains unclear and needs further exploration. Second, this study was conducted only at the in vivo level; however, there are various types of cells present in retinal tissue. Although BRN3a is specifically expressed in RGCs in retinal tissue, the proteins and genes detected by western blot and quantitative real-time PCR (RT-qPCR) in this study represent the overall level of retinal tissue. Future work focusing on the intervention effects of AS-IV on primary cultured RGCs may help further confirm the mechanisms of action of AS-IV.

Overall, our study demonstrated for the first time, to our knowledge, the protective effect of AS-IV on RGCs after TON. In addition, we found the activation of the AMPK-mTOR-ULK pathway after TON and the modulation of this pathway by AS-IV. These findings provide some rationale for the possibility of *Astragalus*, an herbal medicine, in the treatment of optic nerve injury.

Conclusion: In conclusion, our study found that AS-IV can increase the survival rate of RGCs and restore the visual function of TON model rats, which may be related to the increase in autophagy by regulating the AMPK-mTORC1-ULK signaling pathway.

ACKNOWLEDGMENTS

We thank the ophthalmology staff and laboratory technicians in Dongfang Hospital Beijing University of Chinese Medicine for their technical guidance and help in our experiments.

Contributors: Conceptualization: L Liao and J Zhou. Methodology: W Sun, Q Wu, MQ Shang, TY Xia. Software: W Sun, Q Wu. Validation: W Sun, Q Wu. Formal analysis: W Sun, L Liao. Data curation: W Sun. Writing – Original Draft: W Sun, L Liao. Writing – Review & Editing: W Sun, L Liao, J Zhou. Visualization: W Sun. Supervision: L Liao, J Zhou, QP Wei. Project administration: L Liao. Conflict of interest: The authors declare that they have no conflicts of interest. Financial support: This work was supported by "The National Natural Science Foundation of China" (project number 81973909). Ethical statement: This research was approved by the Bioethics Committee of Dongfang Hospital, Beijing University of Chinese Medicine (No. 202,007). Data availability: The data sets used and/or analyzed during the current study are available from the corresponding author on reasonable request. Dr. Wu Sun (wsss55555@sina.com), Dr. Jian Zhou (dfyk55555@126.com;) and Dr. Liang Liao, (b00993@bucm.edu.cn) are co-corresponding authors for this paper.

REFERENCES

1. Chen B, Zhang H, Zhai Q, Li H, Wang C, Wang Y. Traumatic optic neuropathy: a review of current studies. Neurosurg Rev 2022; 45:1895-913. [PMID: 35034261].
2. Karimi S, Arabi A, Ansari I, Shahraki T, Safi S. A Systematic Literature Review on Traumatic Optic Neuropathy. J Ophthalmol 2021; 2021:5553885[PMID: 33728056].
3. Yu-Wai-Man P, Griffiths PG. Steroids for traumatic optic neuropathy. Cochrane Database Syst Rev 2013; 2013:CD006032[PMID: 23771729].
4. Yu-Wai-Man P, Griffiths PG. Surgery for traumatic optic neuropathy. Cochrane Database Syst Rev 2013; 6:CD005024[PMID: 23780732].
5. Li HJ, Sun ZL, Yang XT, Zhu L, Feng DF. Exploring Optic Nerve Axon Regeneration. Curr Neuropharmacol 2017; 15:861-73. [PMID: 28029073].
6. Wu C, Han J, Wu S, Liu C, Zhang Q, Tang J, Liu Z, Yang J, Chen Y, Zhuo Y, Li Y. Reduced Zn^{2+} promotes retinal ganglion cells survival and optic nerve regeneration after injury through inhibiting autophagy mediated by ROS/Nrf2. Free Radic Biol Med 2024; 212:415-32. [PMID: 38134974].
7. Boya P, Esteban-Martínez L, Serrano-Puebla A, Gómez-Sintes R, Villarejo-Zori B. Autophagy in the eye: Development, degeneration, and aging. Prog Retin Eye Res 2016; 55:206-45. [PMID: 27566190].
8. Wen YT, Zhang JR, Kapupara K, Tsai RK. mTORC2 activation protects retinal ganglion cells via Akt signaling after autophagy induction in traumatic optic nerve injury. Exp Mol Med 2019; 51:1-11. [PMID: 31409770].
9. Kim SH, Munemasa Y, Kwong JM, Ahn JH, Mareninov S, Gordon LK, Caprioli J, Piri N. Activation of autophagy in retinal ganglion cells. J Neurosci Res 2008; 86:2943-51. [PMID: 18521932].
10. Rodríguez-Muela N, Germain F, Mariño G, Fitze PS, Boya P. Autophagy promotes survival of retinal ganglion cells after optic nerve axotomy in mice. Cell Death Differ 2012; 19:162-9. [PMID: 21701497].
11. Rodríguez-Muela N, Boya P. Axonal damage, autophagy and neuronal survival. Autophagy 2012; 8:286-8. [PMID: 22301991].
12. Koch JC, Lingor P. The role of autophagy in axonal degeneration of the optic nerve. Exp Eye Res 2016; 144:81-9. [PMID: 26315785].
13. Lin W, Xu G. Autophagy: A Role in the Apoptosis, Survival, Inflammation, and Development of the Retina. Ophthalmic Res 2019; 61:65-72. [PMID: 29694961].
14. Munemasa Y, Kitaoka Y. Autophagy in axonal degeneration in glaucomatous optic neuropathy. Prog Retin Eye Res 2015; 47:1-18. [PMID: 25816798].
15. Alers S, Löffler AS, Wesselborg S, Stork B. Role of AMPK-mTOR-Ulk1/2 in the regulation of autophagy: cross talk, shortcuts, and feedbacks. Mol Cell Biol 2012; 32:2-11. [PMID: 22025673].
16. Li Y, Chen Y. AMPK and Autophagy. Adv Exp Med Biol 2019; 1206:85-108. [PMID: 31776981].
17. Hardie DG, Ross FA, Hawley SA. AMPK: a nutrient and energy sensor that maintains energy homeostasis. Nat Rev Mol Cell Biol 2012; 13:251-62. [PMID: 22436748].
18. Otsubo M, Sase K, Tsukahara C, Fujita N, Arizono I, Tokuda N, Kitaoka Y. Axonal protection by combination of ripasudil and brimonidine with upregulation of p-AMPK in TNF-induced optic nerve degeneration. Int Ophthalmol 2024; 44:173-[PMID: 38598101].
19. Kitaoka Y, Sase K, Tsukahara C, Fujita N, Arizono I, Kogo J, Tokuda N, Takagi H. Axonal Protection by Netarsudil, a ROCK Inhibitor, Is Linked to an AMPK-Autophagy Pathway in TNF-Induced Optic Nerve Degeneration. Invest Ophthalmol Vis Sci 2022; 63:4-[PMID: 34982146].
20. Zhang J, Wu C, Gao L, Du G, Qin X. Astragaloside IV derived from Astragalus membranaceus: A research review on the pharmacological effects. Adv Pharmacol 2020; 87:89-112. [PMID: 32089240].
21. Li H, Zhang Y, Min J, Gao L, Zhang R, Yang Y. Astragaloside IV attenuates orbital inflammation in Graves' orbitopathy through suppression of autophagy. Inflamm Res 2018; 67:117-27. [PMID: 29127443].
22. Song Z, Wei D, Chen Y, Chen L, Bian Y, Shen Y, Chen J, Pan Y. Association of astragaloside IV-inhibited autophagy and mineralization in vascular smooth muscle cells with lncRNA H19 and DUSP5-mediated ERK signaling. Toxicol Appl Pharmacol 2019; 364:45-54. [PMID: 30529164].
23. Zhang J, Zhang W, Ren L, He Y, Mei Z, Feng J, Shi T, Zhang H, Song Z, Jie Z. Astragaloside IV attenuates IL-1β secretion by enhancing autophagy in H1N1 infection. FEMS Microbiol Lett 2020; 367:fnaa007[PMID: 32108899].

24. Wang Z, Wu Y, Pei C, Wang M, Wang X, Shi S, Huang D, Wang Y, Li S, Xiao W, He Y, Wang F. Astragaloside IV pre-treatment attenuates PM2.5-induced lung injury in rats: Impact on autophagy, apoptosis and inflammation. Phytomedicine 2022; 96:153912[PMID: 35026504].

25. Li T, Gao X, Jia R, Sun Y, Ding Y, Wang F, Wang Y. Astragaloside IV inhibits idiopathic pulmonary fibrosis through activation of autophagy by miR-21-mediated PTEN/PI3K/AKT/mTOR pathway. Cell Mol Biol (Noisy-le-grand) 2024; 70:128-36. [PMID: 38430031].

26. Qin L, Wang Y, Liang Y, Li Q, Xie X, Zhang H, Astragaloside IV. Astragaloside IV Alleviates Atorvastatin-Induced Hepatotoxicity via AMPK/SIRT1 Pathway. Pharmacology 2023; 108:74-82. [PMID: 36423574].

27. Li MC, Jia JT, Wang YX, Zhuang YM, Wang HY, Lin ZY, Lu Y, Li MZ, Wang ZJ, Zhao H. Astragaloside IV promotes cerebral tissue restoration through activating AMPK- mediated microglia polarization in ischemic stroke rats. J Ethnopharmacol 2024; 334:118532[PMID: 38972527].

28. Shi G, Chen J, Zhang C, Zhao X, Wang J, Chen R, Xu R, Song D, Zhang X. Astragaloside IV promotes cerebral angiogenesis and neurological recovery after focal ischemic stroke in mice via activating PI3K/Akt/mTOR signaling pathway. Heliyon 2023; 9:e22800[PMID: 38089988].

29. Zhang J, Lu M, Li C, Yan B, Xu F, Wang H, Zhang Y, Yang Y. Astragaloside IV mitigates hypoxia-induced cardiac hypertrophy through calpain-1-mediated mTOR activation. Phytomedicine 2024; 125:155250[PMID: 38295664].

30. Shi YH, Zhang XL, Ying PJ, Wu ZQ, Lin LL, Chen W, Zheng GQ, Zhu WZ. Neuroprotective Effect of Astragaloside IV on Cerebral Ischemia/Reperfusion Injury Rats Through Sirt1/Mapt Pathway. Front Pharmacol 2021; 12:639898[PMID: 33841157].

31. Li M, Li SC, Dou BK, Zou YX, Han HZ, Liu DX, Ke ZJ, Wang ZF. Cycloastragenol upregulates SIRT1 expression, attenuates apoptosis and suppresses neuroinflammation after brain ischemia. Acta Pharmacol Sin 2020; 41:1025-32. [PMID: 32203080].

32. Aghaie F, Moradifar F, Hosseini A. Rapamycin attenuates depression and anxiety-like behaviors through modulation of the NLRP3 pathway in pentylenetetrazole-kindled male Wistar rats. Fundam Clin Pharmacol 2021; 35:1045-54. [PMID: 33930202].

33. Wang W, Zhou Y, Cai Y, Wang S, Shao F, Du J, Fang J, Liu J, Shao X, Liu B, Fang J, Liang Y. Phosphoproteomic Profiling of Rat's Dorsal Root Ganglia Reveals mTOR as a Potential Target in Bone Cancer Pain and Electro-Acupuncture's Analgesia. Front Pharmacol 2021; 12:593043[PMID: 33995007].

34. Rashtiani S, Goudarzi I, Jafari A, Rohampour K. Adenosine monophosphate activated protein kinase (AMPK) is essential for the memory improving effect of adiponectin. Neurosci Lett 2021; 749:135721[PMID: 33582189].

35. Xu W, Li T, Gao L, Zheng J, Yan J, Zhang J, Shao A. Apelin-13/APJ system attenuates early brain injury via suppression of endoplasmic reticulum stress-associated TXNIP/NLRP3 inflammasome activation and oxidative stress in a AMPK-dependent manner after subarachnoid hemorrhage in rats. J Neuroinflammation 2019; 16:247-[PMID: 31791369].

36. Sun W, Chao G, Shang M, Wu Q, Xia Y, Wei Q, Zhou J, Liao L. Optic nerve injury models under varying forces. Int Ophthalmol 2023; 43:757-69. [PMID: 36038691].

37. Odom JV, Bach M, Brigell M, Holder GE, McCulloch DL, Mizota A, Tormene AP. International Society for Clinical Electrophysiology of Vision. ISCEV standard for clinical visual evoked potentials: (2016 update). Doc Ophthalmol 2016; 133:1-9. [PMID: 27443562].

38. Alamusi MT, Matsuo T, Hosoya O, Uchida T. Visual evoked potential in RCS rats with Okayama University-type retinal prosthesis (OURePTM) implantation. J Artif Organs 2017; 20:158-65. [PMID: 28181076].

39. Belforte N, Sande P, de Zavalía N, Knepper PA, Rosenstein RE. Effect of chondroitin sulfate on intraocular pressure in rats. Invest Ophthalmol Vis Sci 2010; 51:5768-75. [PMID: 20574017].

40. Nadal-Nicolás FM, Jiménez-López M, Sobrado-Calvo P, Nieto-López L, Cánovas-Martínez I, Salinas-Navarro M, Vidal-Sanz M, Agudo M. Brn3a as a marker of retinal ganglion cells: qualitative and quantitative time course studies in naive and optic nerve-injured retinas. Invest Ophthalmol Vis Sci 2009; 50:3860-8. [PMID: 19264888].

41. Papadakis M, Hadley G, Xilouri M, Hoyte LC, Nagel S, McMenamin MM, Tsaknakis G, Watt SM, Drakesmith CW, Chen R, Wood MJ, Zhao Z, Kessler B, Vekrellis K, Buchan AM. Tsc1 (hamartin) confers neuroprotection against ischemia by inducing autophagy. Nat Med 2013; 19:351-7. [PMID: 23435171].

42. Qin L, Wang Z, Tao L, Wang Y. ER stress negatively regulates AKT/TSC/mTOR pathway to enhance autophagy. Autophagy 2010; 6:239-47. [PMID: 20104019].

43. Bernard M, Yang B, Migneault F, Turgeon J, Dieudé M, Olivier MA, Cardin GB, El-Diwany M, Underwood K, Rodier F, Hébert MJ. Autophagy drives fibroblast senescence through MTORC2 regulation. Autophagy 2020; 16:2004-16. [PMID: 31931659].

44. Yow YY, Goh TK, Nyiew KY, Lim LW, Phang SM, Lim SH, Ratnayeke S, Wong KH. Therapeutic Potential of Complementary and Alternative Medicines in Peripheral Nerve Regeneration: A Systematic Review. Cells 2021; 10:2194-[PMID: 34571842].

45. Zhang J, Wu C, Gao L, Du G, Qin X. Astragaloside IV derived from Astragalus membranaceus: A research review on the pharmacological effects. Adv Pharmacol 2020; 87:89-112. [PMID: 32089240].

46. Li JQ, Shi YH, Min-Xu , Shi CX, Teng-Wang , Wang TH, Zuo ZF, Liu XZ. Discovery of astragaloside IV against high glucose-induced apoptosis in retinal ganglion cells: Bioinformatics and in vitro studies. Gene 2024; 905:148219[PMID: 38286267].

47. Ben Y, Hao J, Zhang Z, Xiong Y, Zhang C, Chang Y, Yang F, Li H, Zhang T, Wang X, Xu Q. Astragaloside IV Inhibits Mitochondrial-Dependent Apoptosis of the Dorsal Root Ganglion in Diabetic Peripheral Neuropathy Rats Through Modulation of the SIRT1/p53 Signaling Pathway. Diabetes Metab Syndr Obes 2021; 14:1647-61. [PMID: 33883914].

48. Zhang X, Chen J. The mechanism of astragaloside IV promoting sciatic nerve regeneration. Neural Regen Res 2013; 8:2256-65. [PMID: 25206535].

49. Foster KG, Acosta-Jaquez HA, Romeo Y, Ekim B, Soliman GA, Carriere A, Roux PP, Ballif BA, Fingar DC. Regulation of mTOR complex 1 (mTORC1) by raptor Ser863 and multisite phosphorylation. J Biol Chem 2010; 285:80-94. [PMID: 19864431].

50. Jung CH, Jun CB, Ro SH, Kim YM, Otto NM, Cao J, Kundu M, Kim DH. ULK-Atg13-FIP200 complexes mediate mTOR signaling to the autophagy machinery. Mol Biol Cell 2009; 20:1992-2003. [PMID: 19225151].

51. Li MC, Jia JT, Wang YX, Zhuang YM, Wang HY, Lin ZY, Lu Y, Li MZ, Wang ZJ, Zhao H. Astragaloside IV promotes cerebral tissue restoration through activating AMPK- mediated microglia polarization in ischemic stroke rats. J Ethnopharmacol 2024; 334:118532[PMID: 38972527].

52. Qin L, Wang Y, Liang Y, Li Q, Xie X, Zhang H, Astragaloside IV. Astragaloside IV Alleviates Atorvastatin-Induced Hepatotoxicity via AMPK/SIRT1 Pathway. Pharmacology 2023; 108:74-82. [PMID: 36423574].

53. Jin H, Wang L, Li B, Cai C, Ye J, Xia J, Ma S. Astragaloside IV Ameliorates Airway Inflammation in an Established Murine Model of Asthma by Inhibiting the mTORC1 Signaling Pathway. Evid Based Complement Alternat Med 2017; 2017:4037086[PMID: 29234390].

54. Wei R, Liu H, Chen R, Sheng Y, Liu T. Astragaloside IV combating liver cirrhosis through the PI3K/Akt/mTOR signaling pathway. Exp Ther Med 2019; 17:393-7. [PMID: 30651810].

55. Liu G, Wang YH, Zhang T, Li YQ, Chen XY, Dong W, Li W, Miao QX, Qiao WB, Tian HQ, Yin SL. Astragaloside-IV promotes autophagy via the Akt/mTOR pathway to improve cellular lipid deposition. Medicine (Baltimore) 2024; 103:e37846[PMID: 38640324].

56. Ba L, Gao J, Chen Y, Qi H, Dong C, Pan H, Zhang Q, Shi P, Song C, Guan X, Cao Y, Sun H. Allicin attenuates pathological cardiac hypertrophy by inhibiting autophagy via activation of PI3K/Akt/mTOR and MAPK/ERK/mTOR signaling pathways. Phytomedicine 2019; 58:152765[PMID: 31005720].

57. Feng H, Cheng X, Kuang J, Chen L, Yuen S, Shi M, Liang J, Shen B, Jin Z, Yan J, Qiu W. Apatinib-induced protective autophagy and apoptosis through the AKT-mTOR pathway in anaplastic thyroid cancer. Cell Death Dis 2018; 9:1030-[PMID: 30301881].

58. Peng Y, Wang Y, Zhou C, Mei W, Zeng C. PI3K/Akt/mTOR Pathway and Its Role in Cancer Therapeutics: Are We Making Headway? Front Oncol 2022; 12:819128[PMID: 35402264].

59. Yan W, Ma X, Zhao X, Zhang S. Baicalein induces apoptosis and autophagy of breast cancer cells via inhibiting PI3K/AKT pathway in vivo and vitro. Drug Des Devel Ther 2018; 12:3961-72. [PMID: 30510404].

60. Klistorner A, Arvind H, Nguyen T, Garrick R, Paine M, Graham S, O'Day J, Grigg J, Billson F, Yiannikas C. Axonal loss and myelin in early ON loss in postacute optic neuritis. Ann Neurol 2008; 64:325-31. [PMID: 18825673].

61. You Y, Klistorner A, Thie J, Graham SL. Latency delay of visual evoked potential is a real measurement of demyelination in a rat model of optic neuritis. Invest Ophthalmol Vis Sci 2011; 52:6911-8. [PMID: 21791585].

62. You Y, Klistorner A, Thie J, Graham SL. Improving reproducibility of VEP recording in rats: electrodes, stimulus source and peak analysis. Doc Ophthalmol 2011; 123:109-19. [PMID: 21909708].

63. You Y, Thie J, Klistorner A, Gupta VK, Graham SL. Normalization of visual evoked potentials using underlying electroencephalogram levels improves amplitude reproducibility in rats. Invest Ophthalmol Vis Sci 2012; 53:1473-8. [PMID: 22297498].

64. Robson AG, Nilsson J, Li S, Jalali S, Fulton AB, Tormene AP, Holder GE, Brodie SE. ISCEV guide to visual electrodiagnostic procedures. Doc Ophthalmol 2018; 136:1-26. [PMID: 29397523].

65. Ebrahim-Tabar F, Nazari A, Pouramir M, Ashrafpour M, Pourabdolhossein F. Arbutin Improves Functional Recovery and Attenuates Glial Activation in Lysolecethin-Induced Demyelination Model in Rat Optic Chiasm. Mol Neurobiol 2020; 57:3228-42. [PMID: 32506379].

66. Misrielal C, Mauthe M, Reggiori F, Eggen BJL. Autophagy in Multiple Sclerosis: Two Sides of the Same Coin. Front Cell Neurosci 2020; 14:603710[PMID: 33328897].

67. Rangaraju S, Verrier JD, Madorsky I, Nicks J, Dunn WA Jr, Notterpek L. Rapamycin activates autophagy and improves myelination in explant cultures from neuropathic mice. J Neurosci 2010; 30:11388-97. [PMID: 20739560].